Orbital Ordering, New Phases, and Stripe Formation in Doped Layered Nickelates

Takashi Hotta[1] and Elbio Dagotto[2]

[1]*Advanced Science Research Center, Japan Atomic Energy Research Institute, Tokai, Ibaraki 319-1195, Japan*
[2]*National High Magnetic Field Laboratory, Florida State University, Tallahassee, Florida 32306, USA*

(Received 27 January 2004; published 2 June 2004)

Ground-state properties of layered nickelates are investigated based on the orbital-degenerate Hubbard model coupled with lattice distortions, by using numerical techniques. The Néel state composed of spin $S = 1$ ions is confirmed in the undoped limit $x = 0$. At $x = 1/2$, novel antiferromagnetic states, called CE- and E-type phases, are found by increasing the Hund's coupling. $(3x^2 - r^2/3y^2 - r^2)$-type orbital ordering is predicted to occur in a checkerboard-type charge-ordered state. At $x = 1/3$, *both* Coulombic and phononic interactions are found to be important, since the former stabilizes the spin stripe, while the latter leads to the striped charge order.

DOI: 10.1103/PhysRevLett.92.227201 PACS numbers: 75.30.Kz, 71.10.Fd, 75.47.Lx, 75.50.Ee

The existence and origin of "striped" structures continues attracting considerable attention in the research field of transition-metal oxides [1]. In a system with dominant electron-electron repulsion, the Wigner-crystal state should be stabilized, but in real materials more complicated nonuniform charge structures have been found. In Nd-based lightly doped cuprates, neutron scattering experiments revealed incommensurate spin structures [2] where antiferromagnetic (AFM) spin stripes are periodically separated by domain walls of holes. In $La_{2-x}Sr_xCuO_4$, dynamical stripes are believed to exist along vertical or horizontal directions (Cu-O bond direction) [3]. In nickelates, the charge-ordered stripes are along the diagonal direction [4]. In manganites, evidence for striped charge ordering also along the diagonal direction has been reported in the AFM phase for $x > 1/2$ [5], while short-range diagonal stripe correlations have been found in the ferromagnetic (FM) phase at $x < 1/2$ [6].

In general, stripes can be classified into metallic or insulating. In $La_{2-x}Sr_xCuO_4$, the dynamical stripes exhibit metallic properties, but they are easily pinned by lattice effects and impurities. In $La_{1.6-x}Nd_{0.4}Sr_xCuO_4$, stripes along the bond direction are pinned by lattice distortions [1], but they are still metallic. Intuitively, vertical or horizontal stripes could be associated with the formation of "rivers of holes," to prevent individual charges from fighting against the AFM background [7]. Such stripes should be metallic, even if they are pinned, since they are induced by the optimization of hole motion between nearest-neighbor Cu sites via oxygens.

However, in the diagonal stripes observed in manganites and nickelates, charges are basically localized, indicating that such insulating stripes are *not* determined just by the optimization of the hole motion. In the FM state of manganites, the hole movement is already optimal and, naively, charges should not form stripes. Obviously, an additional effective local potential must be acting to confine electrons into stripes. If such a potential originates in lattice distortions, it is expected to occur along the bond direction to avoid energy loss due to the conflict between neighboring lattice distortions sharing the same oxygens. Then, static stripes stabilized by lattice distortions tend to occur along the *diagonal* direction, as shown in the stripes of the FM phase of manganites, stabilized by Jahn-Teller (JT) distortions [8].

In simple terms, vertical or horizontal stripes in cuprates can be understood by the competition between Coulomb interaction and hole motion, while diagonal stripes are better explained as a consequence of a robust electron-lattice coupling. However, a difficulty has been found for theoretical studies of stripe formation in doped nickelates, since both Coulomb interaction and electron-lattice coupling appear to be important. Since the Ni^{2+} ion has two electrons in the e_g orbitals, on-site Coulomb interactions certainly play a crucial role to form spins $S = 1$. When holes are doped, one electron is removed and another remains in the e_g orbitals, indicating that the hole-doped site should become JT active. Then, in hole-doped nickelates *both* Coulombic and phononic interactions could be of relevance, a fact not considered in previous theoretical investigations.

In this Letter, charge ordering in doped nickelates is investigated based on the orbital-degenerate Hubbard model coupled to lattice distortions, using numerical techniques. After confirming the Néel state composed of $S = 1$ spins at $x = 0$, both cases $x = 1/2$ and $1/3$ will be analyzed. At $x = 1/2$, novel AFM phases called CE and E types have been unveiled, which are consistent with experimental results. Further including the JT-type cooperative distortion, a $(3x^2 - r^2/3y^2 - r^2)$-type orbital ordering is predicted. For $x = 1/3$, an incommensurate spin structure is induced by the Coulombic model, including the level splitting between e_g orbitals, but the charge stripe does not appear. To reproduce simultaneously spin and charge stripes, it is important to include the strong coupling of e_g electrons to lattice distortions, originating in the in-plane oxygen motions.

The model for nickelates includes three important ingredients: The kinetic motion of e_g electrons, Coulomb interactions among e_g electrons, and electron-lattice

couplings between e_g electrons and distortions of the NiO_6 octahedra. Note that the electron-lattice term is divided into couplings for the apical and in-plane oxygen motions. In layered nickelates, all NiO_6 octahedra are significantly elongated along the c axis, splitting the e_g orbitals. This splitting from apical oxygens should be included explicitly from the start and, then, the in-plane motion should be studied. The Hamiltonian H is given by

$$H = -\sum_{\mathbf{i}\mathbf{a}\gamma\gamma'\sigma} t^{\mathbf{a}}_{\gamma\gamma'} d^{\dagger}_{\mathbf{i}\gamma\sigma} d_{\mathbf{i}+\mathbf{a}\gamma'\sigma} + \Delta \sum_{\mathbf{i}} (n_{\mathbf{i}\mathrm{a}} - n_{\mathbf{i}\mathrm{b}})/2 + U \sum_{\mathbf{i},\gamma} n_{\mathbf{i}\gamma\downarrow} n_{\mathbf{i}\gamma\uparrow} + J \sum_{\mathbf{i},\sigma,\sigma'} d^{\dagger}_{\mathbf{i}\mathrm{a}\sigma} d^{\dagger}_{\mathbf{i}\mathrm{b}\sigma'} d_{\mathbf{i}\mathrm{a}\sigma'} d_{\mathbf{i}\mathrm{b}\sigma} + U' \sum_{\mathbf{i}} n_{\mathbf{i}\mathrm{a}} n_{\mathbf{i}\mathrm{b}} + J' \sum_{\mathbf{i},\gamma\neq\gamma'} d^{\dagger}_{\mathbf{i}\gamma\uparrow} d^{\dagger}_{\mathbf{i}\gamma\downarrow} d_{\mathbf{i}\gamma'\downarrow} d_{\mathbf{i}\gamma'\uparrow}, \quad (1)$$

where $d_{\mathbf{i}\mathrm{a}\sigma}$ ($d_{\mathbf{i}\mathrm{b}\sigma}$) is the annihilation operator for an e_g electron with spin σ in the $d_{x^2-y^2}$ ($d_{3z^2-r^2}$) orbital at site $\mathbf{i}$, $n_{\mathbf{i}\gamma\sigma} = d^{\dagger}_{\mathbf{i}\gamma\sigma} d_{\mathbf{i}\gamma\sigma}$, $n_{\mathbf{i}\gamma} = \sum_{\&\mathrm{sigma};} n_{\mathbf{i}\gamma\sigma}$, $\mathbf{a}$ is the vector connecting nearest-neighbor sites, and $t^{\mathbf{a}}_{\gamma\gamma'}$ is the nearest-neighbor hopping amplitude between γ and γ' orbitals along the $\mathbf{a}$ direction, given by $t^{\mathbf{x}}_{\mathrm{aa}} = -\sqrt{3} t^{\mathbf{x}}_{\mathrm{ab}} = -\sqrt{3} t^{\mathbf{x}}_{\mathrm{ba}} = 3t^{\mathbf{x}}_{\mathrm{bb}} = 3t/4$ for the x direction and $t^{\mathbf{y}}_{\mathrm{aa}} = \sqrt{3} t^{\mathbf{y}}_{\mathrm{ab}} = \sqrt{3} t^{\mathbf{y}}_{\mathrm{ba}} = 3t^{\mathbf{y}}_{\mathrm{bb}} = 3t/4$ for the y direction [9]. Hereafter, t is the energy unit. In the second term, Δ (>0) is the level splitting between a and b orbitals. In the Coulomb interaction terms, U (U') is the intraorbital (interorbital) Coulomb interaction, J is the interorbital exchange interaction, and J' is the pair-hopping amplitude between different orbitals. Because of the relations $J = J'$ and $U = U' + J + J'$, the independent parameters are U' and J, with $U' > J$ [9]. The calculations are all carried out using standard exact-diagonalization techniques. It is crucial to use this kind of *unbiased* methods for this first study that includes both Coulomb and lattice effects, even if the technique restricts us to small N-site clusters.

First, consider the undoped case. The calculation is done for an 8-site tilted cluster, equivalent in complexity to a 16-site lattice for the single-band Hubbard model. Since at all sites the two orbitals are occupied due to the Hund's rule coupling, the JT distortions are not active and it is possible to grasp the essential ground-state properties using H. In Fig. 1(a), the Fourier transform of spin correlations is shown vs Δ, where $S(\boldsymbol{q}) = (1/N)\sum_{\mathbf{i},\mathbf{j}} e^{i\boldsymbol{q}\cdot(\mathbf{i}-\mathbf{j})} \langle S^z_{\mathbf{i}} S^z_{\mathbf{j}} \rangle$, with $S^z_{\mathbf{i}} = \sum_{\gamma} (d^{\dagger}_{\mathbf{i}\gamma\uparrow} d_{\mathbf{i}\gamma\uparrow} - d^{\dagger}_{\mathbf{i}\gamma\downarrow} d_{\mathbf{i}\gamma\downarrow})/2$. As expected, a robust (π, π) peak can be observed for $\Delta \lesssim 3$, suggesting that the AFM phase is stabilized by superexchange interactions. The rapid decrease of $S(\pi, \pi)$ for $\Delta \gtrsim 3$ is understood by comparing the energies for local triplet and singlet states, as shown in Fig. 1(b). The ground-state properties change at $U' - J = U - \Delta$, leading to $\Delta = 3J$ for the transition. The spin structure at $x = 0$ is schematically shown in Fig. 1(c).

Let us turn our attention to the case $x = 1/2$. The 8-site tilted lattice is again used for the analysis, and the phase diagram Fig. 2(a) is obtained for $\Delta = 0.5$ [10]. Increasing J, an interesting transformation from AFM to FM phases

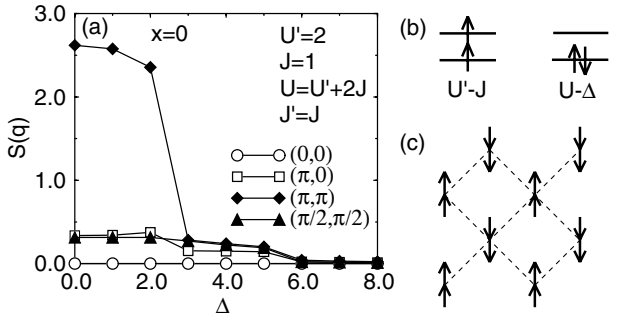

FIG. 1. (a) Spin correlation $S(\boldsymbol{q})$ vs Δ for $x = 0$. (b) Two kinds of local e_g-electron arrangements for $x = 0$. (c) AFM spin pattern theoretically determined for $\Delta \lesssim 3$.

is found. This is natural, since at large J the system has a formal similarity with manganite models, where kinetic-energy gains lead to ferromagnetism, while at small J the magnetic energy dominates. However, between the G-type AFM for $J \approx 0$ and FM phase for $J \approx U'$, unexpected states appear which are mixtures of FM and AFM phases, due to the competition between kinetic and magnetic energies. Typical spin correlations $S(\boldsymbol{q})$ are shown in Fig. 2(b). Note that peaks at $\boldsymbol{q} = (\pi, 0)$ and $(\pi/2, \pi/2)$ indicate "C"- and "E"-type spin structures, respectively (the notation is borrowed from the Mn-oxide context [9]). Double peaks at $\boldsymbol{q} = (\pi, 0)$ and $(\pi/2, \pi/2)$ denote the CE-type structure, frequently observed in half-doped manganites [11]. In half-doped nickelates, the CE phase is expressed as a mixture of types (I) and (II) in Fig. 2(c), depending on the positions of the $S = 1$ and $S = 1/2$ sites, although the "zigzag" FM chain structure is common for both types. The E-type phase is also depicted in Fig. 2(c). Note that the charge correlation always exhibits a peak at $\boldsymbol{q} = (\pi, \pi)$ (not shown here), indicating the checkerboard-type charge ordering.

In experimental results, a peak at $(\pi/2, \pi/2)$ in $S(\boldsymbol{q})$ has been reported [4], suggesting an AFM pair of $S = 1$ spins *across* the singly occupied sites with holes. Moreover, the checkerboard-type charge ordering has been experimentally observed [4]. Thus, the spin-charge patterns of CE (II) and E types are consistent with the experimental results. Our phase diagram has a robust region with a peak at $(\pi/2, \pi/2)$, both for CE- and E-type phases, although the CE phase exhibits an extra peak at $(\pi, 0)$. Whether the E or CE phases are present in nickelates can be studied experimentally in the future by searching for this $(\pi, 0)$ peak. Note that if diffuse scattering experiments detect the AF correlation *along* the hole stripe, as has been found at $x = 1/3$ [12], the CE (II) type may be the only possibility. Summarizing, the spin-charge structure in $x = 1/2$ experiments can be understood within the Hamiltonian H by assuming a relatively large J.

Consider now the effect of in-plane oxygen motion (apical oxygen motions have already been included as an e_g-level splitting). Assuming that oxygens move along

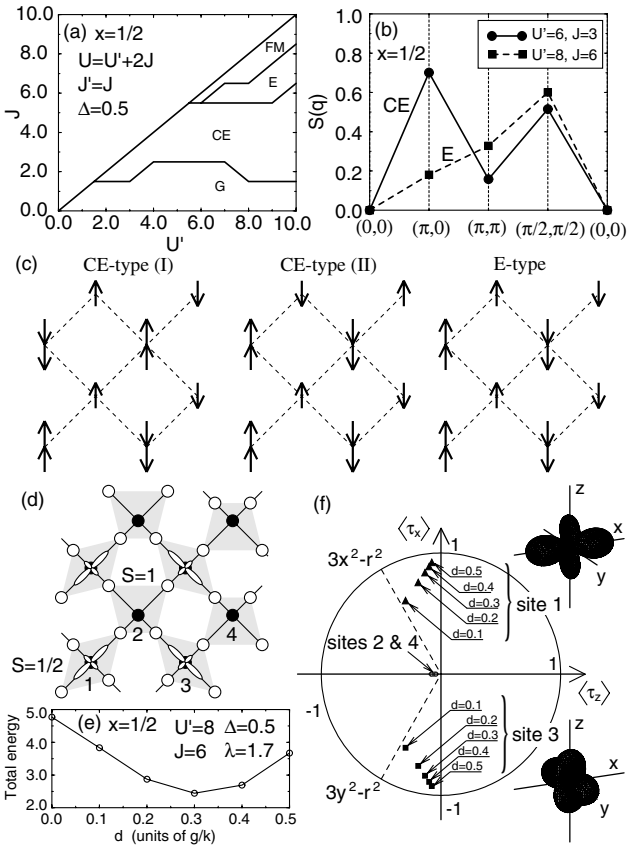

FIG. 2. (a) Ground-state phase diagram at $x = 1/2$. (b) $S(\boldsymbol{q})$ for the CE- and E-type phases, at the couplings indicated. (c) Spin and charge patterns for the CE- and E-type phases. These are schematic views, since local charge densities in practice are not exactly 1 and 2. (d) Numerically obtained cooperative distortion pattern for an 8-site lattice at $x = 1/2$. Solid and open circles indicate Ni and O ions, respectively. Open symbols indicate e_g orbitals in the optimized state. (e) Total ground-state energy vs d for $x = 1/2$. (f) Orbital densities $\langle\tau_{z\mathbf{i}}\rangle$ and $\langle\tau_{x\mathbf{i}}\rangle$ for sites 1–4. See (d) for the site labels. Optimized orbitals at $d = 0.3$ for sites 1 and 3 are also shown.

the Ni-O bond direction, the extra electron-phonon coupling term is written as

$$H_{\mathrm{eph}} = g\sum_{\mathbf{i}}[-Q_{1\mathbf{i}}(n_{\mathbf{i}a} + n_{\mathbf{i}b}) + Q_{2\mathbf{i}}\tau_{x\mathbf{i}} + Q_{3\mathbf{i}}\tau_{z\mathbf{i}}] + (k/2)\sum_{\mathbf{i}}(\beta Q_{1\mathbf{i}}^2 + Q_{2\mathbf{i}}^2 + Q_{3\mathbf{i}}^2), \quad (2)$$

where g is the electron-lattice coupling constant, $Q_{1\mathbf{i}}$ is the breathing-mode distortion, $Q_{2\mathbf{i}}$ and $Q_{3\mathbf{i}}$ are, respectively, the $(x^2 - y^2)$- and $(3z^2 - r^2)$-type JT distortions, $\tau_{x\mathbf{i}} = \sum_\sigma (d^\dagger_{\mathbf{i}a\sigma} d_{\mathbf{i}b\sigma} + d^\dagger_{\mathbf{i}b\sigma} d_{\mathbf{i}a\sigma})$, and $\tau_{z\mathbf{i}} = \sum_\sigma (d^\dagger_{\mathbf{i}a\sigma} d_{\mathbf{i}a\sigma} - d^\dagger_{\mathbf{i}b\sigma} d_{\mathbf{i}b\sigma})$. The second term is the quadratic potential for adiabatic distortions, where k is the spring constant for the JT mode and β is the spring-constant ratio for breathing and JT modes. From our experience in manganites, this ratio is here fixed to $\beta = 2$ [13].

Since all oxygens are shared by adjacent NiO_6 octahedra, the distortions are *not independent*. To consider such cooperative effect, in principle, the O-ion displacements should be optimized. However, in practice it is not feasible to perform both the Lanczos diagonalization and the optimization of all oxygen positions for 6- and 8-site clusters. In the actual calculations, $Q_{1\mathbf{i}}$, $Q_{2\mathbf{i}}$, and $Q_{3\mathbf{i}}$ are expressed by a single parameter d, for the shift of the O-ion coordinate. Note that the unit of d is g/k, typically 0.1–0.3 Å. Then, the total energy is evaluated as a function of d to find the minimum energy state. Repeating these calculations for several distortion patterns, it is possible to deduce the optimal state.

After several trials, the optimal distortion at $x = 1/2$ is shown in Fig. 2(d). The diagonalization has been performed at several values of d on the 8-site distorted lattice and the minimum in the total energy is found at $d = 0.3$ [Fig. 2(e)]. Here, the dimensionless coupling constant λ is defined as $\lambda = g/\sqrt{kt}$. As mentioned above, even without H_{eph}, the checkerboard-type charge ordering has been obtained, but the peak at $\boldsymbol{q} = (\pi, \pi)$ significantly grows due to the effect of lattice distortions. Note that the distortion pattern in Fig. 2(d) is essentially the same as

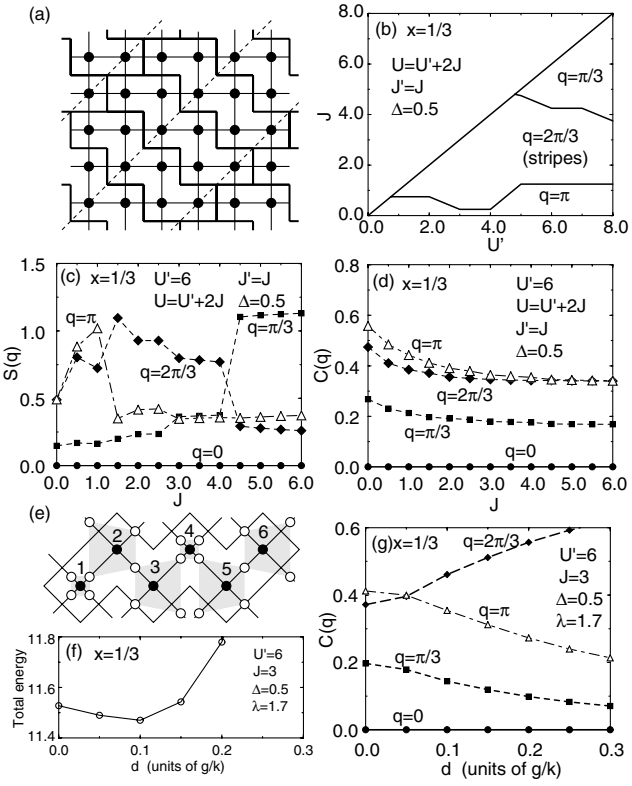

FIG. 3. (a) Zigzag 6-site cluster covering the 2D lattice. Solid circles denote Ni ions, and dashed lines indicate hole positions. (b) Phase diagram at $x = 1/3$. Each phase is characterized by the momentum that shows a peak in $S(q)$. (c) $S(q)$ and (d) $C(q)$ vs J for $U' = 6$ and $\Delta = 0.5$. (e) Cooperative distortion pattern for the zigzag 6-site cluster at $x = 1/3$. (f) Total ground-state energy and (g) $C(q)$ vs d for $x = 1/3$.

that for half-doped manganites. This is quite natural, since JT active and inactive ions exist bipartitely also for half-doped nickelates. Then, due to this JT-type distortion *orbital ordering for half-doped nickelates* is predicted, as schematically shown in Fig. 2(d). The shapes of orbitals are determined from the orbital densities, $\langle\tau_{z\mathbf{i}}\rangle$ and $\langle\tau_{x\mathbf{i}}\rangle$ [Fig. 2(f)]. The well-known alternate pattern of $3x^2 - r^2$ and $3y^2 - r^2$ orbitals in half-doped manganites is denoted by dashed lines. Increasing d, the shape of orbitals deviates from $3x^2 - r^2$ and $3y^2 - r^2$, but it is still characterized by the orbitals elongating along the x and y directions [see insets of Fig. 2(f)]. It would be very interesting to search for orbital ordering in half-doped nickelates, using the resonant x-ray scattering technique.

Now let us move to the case $x = 1/3$. If the actual expected stripe structure at $x = 1/3$ is faithfully considered [4], it is necessary to analyze, at least, a 6×6 cluster. However, such a large-size cluster with orbital degeneracy cannot be treated exactly due to the exponential growth of the Hilbert space with cluster size. Then, a covering of the two-dimensional (2D) lattice using zigzag 6-site clusters is considered [Fig. 3(a)] by assuming a periodic structure along the diagonal direction. The phase diagram obtained by analyzing the zigzag 6-site cluster for H is in Fig. 3(b). Typical spin and charge correlations are in Figs. 3(c) and 3(d), where $C(\boldsymbol{q}) = (1/N) \times \sum_{\mathbf{i},\mathbf{j}} e^{i\boldsymbol{q}\cdot(\mathbf{i}-\mathbf{j})}\langle(n_{\mathbf{i}} - \langle n\rangle)\cdot(n_{\mathbf{j}} - \langle n\rangle)\rangle$, with $n_{\mathbf{i}} = \sum_{\gamma} n_{\mathbf{i}\gamma}$.

Since the momentum q is defined along the zigzag direction, the phase labeled by $q = 2\pi/3$ in Fig. 3(b) denotes an *incommensurate AFM phase* with the proper spin stripe structure. The phase labeled by $q = \pi/3$ indicates a spin spiral state, which will eventually turn to the FM phase in the thermodynamic limit. Thus, the spin stripe phase appears between the commensurate AFM- and FM-like phases, similar to the case of $x = 1/2$. However, as seen in Fig. 3(d), $C(q)$ in the spin stripe phase does not show the striped charge structure ($q = 2\pi/3$). Rather, bipartite charge ordering characterized by a peak at $q = \pi$ still remains. Namely, the Hamiltonian H can explain the spin stripe, but does not reproduce the striped charge ordering at $x = 1/3$, indicating the importance of H_{eph}.

Consider now the effect of H_{eph} for $x = 1/3$. After evaluating total ground-state energies for several kinds of distortions, the pattern in Fig. 3(e) has been found to provide the optimal state at $x = 1/3$. This type of distortion induces a spatial modulation of the level splitting as $-\delta_1/2 = \delta_2 = \delta_3 = -\delta_4/2 = \delta_5 = \delta_6$ [14], where $\delta_{\mathbf{i}}$ is the level splitting caused by the in-plane oxygen motions, and the site numbers are in Fig. 3(e). The minimum energy is found at $d = 0.1$ [Fig. 3(f)]. The modulation of level splitting stabilizes the striped charge ordering characterized by a $q = 2\pi/3$ peak in $C(q)$ [Fig. 3(g)].

Note that $(3x^2 - r^2/3y^2 - r^2)$-type orbital ordering does not occur in Fig. 3(e). Phenomenologically, such orbital ordering tends to appear in a hole pair separated by one site, the unit of the "bistripe" of manganites [5]. However, such a bistripe-type ordering contradicts the $x = 1/3$ striped charge ordering, and the bistripe-type solution was found to be unstable in these calculations. One may consider other distortion patterns which satisfy both $(3x^2 - r^2/3y^2 - r^2)$-type orbital and striped charge ordering, but in such distortions no energy minimum was obtained for $d > 0$. After several trials, Fig. 3(e) has provided the most optimal state.

Summarizing, possible spin, charge, *and* orbital structures of layered nickelates have been discussed based on the e_g-orbital degenerate Hubbard model coupled with lattice distortions. To understand the nickelate stripes, *both Hund's rule interaction and electron-lattice coupling appear essentially important.* At $x = 1/2$, $(3x^2 - r^2/3y^2 - r^2)$-type orbital ordering similar to that in half-doped manganites is predicted. Even FM phases could be stabilized by chemically altering the carrier's bandwidth. For $x = 1/3$, a spatial modulation in level splitting plays an important role for stripe formation.

The authors thank M. Matsuda, J. Tranquada, and H. Yoshizawa for discussions. T. H. is supported by a Priority-Areas Grant from the Ministry of Education, Culture, Sports, Science, and Technology of Japan. E. D. is supported by the NSF Grants No. DMR-0122523 and No. 0312333.

[1] J. M. Tranquada *et al.*, Nature (London) **375**, 561 (1995); H. A. Mook *et al.*, Nature (London) **404**, 729 (2002).
[2] S.-W. Cheong *et al.*, Phys. Rev. Lett. **67**, 1791 (1991); T. E. Mason *et al.*, *ibid.* **68**, 1414 (1992); T. R. Thurston *et al.*, Phys. Rev. B **46**, 9128 (1992).
[3] For $x < 0.02$, the spin-glass phase exhibits a diagonal spin modulation. See M. Matsuda *et al.*, Phys. Rev. B **65**, 134515 (2003).
[4] J. M. Tranquada *et al.*, Phys. Rev. Lett. **73**, 1003 (1994); V. Sachan *et al.*, Phys. Rev. B **51**, 12 742 (1995); H. Yoshizawa *et al.*, Phys. Rev. B **61**, R854 (2000); R. Kajimoto *et al.*, Phys. Rev. B **67**, 014511 (2003).
[5] S. Mori *et al.*, Nature (London) **392**, 473 (1998).
[6] P. Dai *et al.*, Phys. Rev. Lett. **85**, 2553 (2000); C. P. Adams *et al.*, *ibid.* **85**, 3954 (2000).
[7] V. J. Emery *et al.*, Phys. Rev. B **56**, 6120 (1997); C. Buhler *et al.*, Phys. Rev. Lett. **84**, 2690 (2000); A. L. Malvezzi and E. Dagotto, Phys. Rev. B **63**, 140409 (2001).
[8] T. Hotta *et al.*, Phys. Rev. Lett. **86**, 4922 (2001).
[9] E. Dagotto *et al.*, Phys. Rep. **344**, 1 (2001).
[10] Since Δ of nickelates is half that of cuprates, from the lattice constants for CuO_6 and NiO_6 octahedra, it is reasonable to select $\Delta/t = 0.5$.
[11] Y. Murakami *et al.*, Phys. Rev. Lett. **80**, 1932 (1998).
[12] A. T. Boothroyd *et al.*, Phys. Rev. Lett. **91**, 257201 (2003).
[13] T. Hotta *et al.*, Phys. Rev. B **60**, R15 009 (1999).
[14] This breathing-mode modulation is consistent with experimental results. See J. M. Tranquada *et al.*, Phys. Rev. B **52**, 3581 (1995).